

# Ultrahigh Linearity of the Magnetic-Flux-to-Voltage Response of Proximity-Based Mesoscopic Bi-SQUIDS

Giorgio De Simoni<sup>1,\*</sup>, Lorenzo Cassola<sup>1,2</sup>, Nadia Ligato,<sup>1</sup>  
Giuseppe C. Tettamanzi<sup>1,3</sup>, and Francesco Giazotto<sup>1,†</sup>

<sup>1</sup>*NEST, Istituto Nanoscienze—CNR and Scuola Normale Superiore, Pisa I-56127, Italy*

<sup>2</sup>*Department of Physics “E. Fermi,” Università di Pisa, Largo Pontecorvo 3, Pisa I-56127, Italy*

<sup>3</sup>*Institute of Photonics and Advanced Sensing and School of Physical Sciences, The University of Adelaide, Adelaide, SA 5005, Australia*

(Received 14 January 2022; revised 18 March 2022; accepted 7 June 2022; published 28 July 2022; corrected 17 August 2022)

Superconducting double-loop interferometers (bi-SQUIDS) have been introduced to produce magnetic flux sensors specifically designed to exhibit an ultrahighly linear voltage response as a function of the magnetic flux. These devices are very important for quantum sensing and for signal processing of signals oscillating in the radio-frequency range of the electromagnetic spectrum. Here, we report an Al double-loop bi-SQUID based on proximitized mesoscopic Cu Josephson junctions. Such a scheme provides an alternative fabrication approach to conventional tunnel-junction-based interferometers, where the junction characteristics and, consequently, the magnetic-flux-to-voltage and magnetic-flux-to-critical-current device responses can be largely and easily tailored by the geometry of the metallic weak links. We discuss the performance of such sensors by showing a full characterization of the device switching current and voltage drop versus the magnetic flux for operation temperatures ranging from 30 mK to approximately 1 K. The figures of merit of the transfer function and of the total harmonic distortion are also discussed. The latter provides an estimate of the linearity of the flux-to-voltage device response, which attains values as large as 45 dB. Such a result lets us foresee a performance already on par with that achieved in conventional tunnel-junction-based bi-SQUIDS arrays composed of hundreds of interferometers.

DOI: 10.1103/PhysRevApplied.18.014073

## I. INTRODUCTION

Superconducting quantum interference devices (SQUIDs) provide the reference standard for magnetic flux detectors [1–7] and for the measurement of all those physical quantities that can be transduced from magnetic to electrical properties. In this sense, SQUIDs can be integrated into larger systems and used for signal-processing applications [8]. In their simplest implementation, direct-current (dc) SQUIDs comprise a pair of Josephson junctions (JJs) [9] closed in a superconducting ring, the critical current of which is modulated by the magnetic flux threading the loop with a periodicity equal to the magnetic flux quantum  $\phi_0 = h/2e$  [1,2,10,11]. Because the sensing abilities of dc SQUIDs are directly linked to the basic principles of quantum mechanics, they can already approach the quantum limits of sensing in their conventional implementations [1]. However, dc SQUIDs are characterized by poor performance in terms of linearity and dynamic range: these issues

have been routinely circumvented by means of a specific optimization that, at the cost of a drastic reduction of the operation bandwidth, is implemented through the introduction of external feedback loops [1,3,7]. On the other hand, high-frequency open-loop SQUID amplifiers, that have been demonstrated to be suitable for applications up to the gigahertz range [12–21], exhibit severe limitations due to significant nonlinear distortion [14]. Mitigation of these restrictions has been achieved due to the introduction of a class of superconducting interferometers containing a third JJ connected in parallel with the inductance loop of a dc SQUID. In such devices, called bi-SQUIDS [8,22–24], the third JJ is used as additional nonlinear element operating in parallel to compensate for the nonlinear response of the dc SQUID, resulting in a highly linear voltage response [8,22,23]. Despite such promising premises, due to their large junction area and inductance, Nb bi-SQUIDS with shunted Josephson tunnel junctions [25] have shown a nonideal voltage response, with a linearity performance far from the expected one [8]. Instead, Nb bi-SQUIDS based on arrays of different numbers of interferometers, ranging between tens and hundreds of unit cells, have proven to be extremely effective for low-noise signal amplification and

\*giorgio.desimoni@sns.it

†francesco.giazotto@sns.it

magnetic field sensing, exhibiting excellent performance in terms of the linearity of the flux-to-voltage response [22,26,27].

Although the great majority of superconducting interferometers used in commercial applications exploit superconductor-insulator-superconductor (*S-I-S*) JJs, the dc Josephson effect can be observed in a broad variety of systems [28], such as in Dayem bridges [29,30], or in weak links based on a semiconductor [31–33] or a normal metal [34] sandwiched between a pair of superconducting leads (*S-N-S* JJs). *S-N-S* junctions support a nondissipative current due to the proximity effect [35] stemming from the building of Andreev bound states in the *N* region [36,37], which lends the superconducting correlations to the electron gas in clean electric contact with the *S* leads. *S-N-S* JJs have gained growing interest in device physics due to their negligible parasitic capacitance and, even more so, to a convenient and reproducible fabrication process, which allows their critical current and the functional form of their current-phase relation [38,39] to be tailored to specific application needs just through the geometry of the weak link. In conventional tunnel-junction bi-SQUIDs, the linearity of the magnetic-field-to-voltage response can be controlled through the ratios of the critical current of the three JJs [24]. These are set during fabrication by properly choosing the junction areas and through the opacity of the tunnel barriers. These parameters also affect the capacity of the junctions. Similarly, in bi-SQUIDs based on *S-N-S* weak links, the critical currents can be regulated by setting the section and length of the weak links and the size of the overlapping area of the *S* and *N* regions. Differently from the tunnel case, however, the capacitance of the *S-N-S* junction always remains negligible. This makes such an approach particularly useful whenever a large junction capacitance is expected to be detrimental or in those applications where it is necessary to disentangle its value from the other parameters of the junction. Furthermore, the critical current of *S-N-S* JJs can be tuned down to zero by the application of a gate voltage [40,41]. This last feature, which has not been demonstrated so far for tunnel junctions, might be exploitable in order to vary and improve the device performance during its operation [42]. In this work, we demonstrate the operation of Al bi-SQUIDs in which three nanojunctions are implemented through proximitized mesoscopic Cu weak links. Although their relatively low critical temperature, Al is chosen due to its efficient proximation capability over copper [40,41], we emphasize that this scheme can be easily exploited in a higher-temperature working range simply by replacing the Al with a higher-critical-temperature superconductor, such as Nb [43] or V [44,45]. Hence, the realization of this identical technology in regimes of operation ranging between 4 K and 10 K is achievable. Finally, our devices exhibit very promising flux-to-voltage response characteristics which, in this prototypical realization, lets us foresee performance already

on par with that of bi-SQUID arrays composed of hundreds of tunnel-junction-based interferometers.

## II. RESULTS AND DISCUSSION

A false-colored scanning electron micrograph of a representative *S-N-S* bi-SQUID is shown in Fig. 1(a): it consists of a main 100-nm-thick Al (colored in blue) and

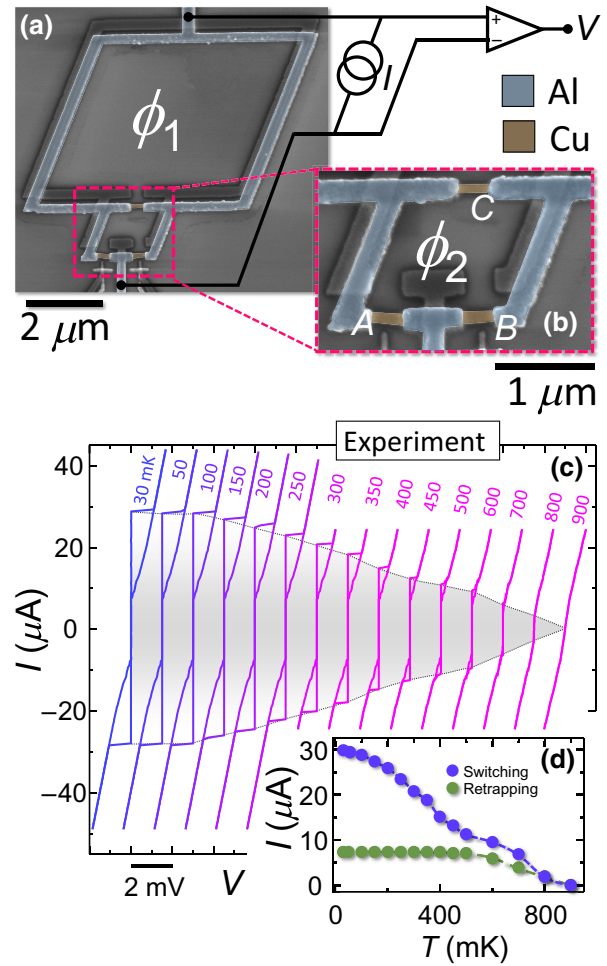


FIG. 1. A proximity-based all-metallic bi-SQUID. (a) A false-color scanning electron micrograph of a representative double-loop dc superconducting quantum interference device (bi-SQUID) based on superconductor–normal-metal–superconductor (*S-N-S*) proximity Josephson junctions. The Al interferometer ring is colored in blue. The Cu Josephson weak links are colored in brown. The four-wire electrical setup is also shown. (b) A higher-magnification false-color scanning electron micrograph of the second loop of the bi-SQUID. The Cu weak links are labeled as *A*, *B*, and *C*. (c) The current (*I*) versus voltage (*V*) forward and backward characteristics of a representative bi-SQUID at selected temperatures between 30 mK and 900 mK and at zero magnetic flux. The curves are horizontally offset for clarity. The *I*-*V* nondissipative region is shaded in gray. (d) The switching (violet) and retrapping (green) current of the same device as in (a) versus the temperature *T*.

superconducting loop (loop 1), spanning an area of approximately  $30 \mu\text{m}^2$ , closed on an approximately 10 times smaller loop (loop 2) and comprising three 20-nm-thick and 320-nm-long Cu weak links [brown colored in Fig. 1(b)] labeled *A*, *B*, and *C*, according to the notation used in Fig. 1(b). Junctions *A* and *B* are approximately 120 nm wide, while junction *C* is 90 nm wide. The latter parameter value is chosen in order to limit the critical current of junction *C* around approximately 0.75 of that of junctions *A* and *B*, i.e., within the range where a maximization of the linearity performance of the interferometer is expected. All the weak links fall in the diffusive regime and within the long-junction limit. Indeed, the Thouless energy of the junctions,  $E_{\text{Th}}$ , is  $E_{\text{Th}} = \hbar D/l^2 \simeq 50 \mu\text{eV} \ll \Delta_{\text{Al}} \simeq 180 \mu\text{eV}$ , where  $D \simeq 0.008 \text{ m}^2/\text{s}$  is the Cu diffusion coefficient [40],  $l$  is the weak-link length, and  $\Delta_{\text{Al}}$  is the superconducting energy gap of the Al banks. Long *S-N-S* junctions have a current-phase relation that is sinusoidal. This allows us to predict the device behavior through a simple and compact resistively shunted junction (RSJ) model, thereby facilitating the interpretation of the experimental data for the design of future devices. Further details of the fabrication process are given in Appendix A 1.

Figure 1(c) shows the  $I$ - $V$  characteristics of a bi-SQUID measured as a function of the bath temperature, ranging from 30 mK to 900 mK. A scheme of the four-wire electrical setup is shown in Fig. 1(a). For temperatures lower than approximately 800 mK, the  $I$ - $V$  curves show the Josephson effect, with the switching  $I_S$  and the retrapping current [46,47]  $I_R$  reaching approximately 30  $\mu\text{A}$  and approximately 7  $\mu\text{A}$ , respectively, at 30 mK. At the same temperature, the normal-state resistance  $R_N$  is approximately  $40\Omega$ .  $I_S$  and  $I_R$  are plotted versus the bath temperature ( $T$ ) in Fig. 1(d).

The measurement of the  $I$ - $V$  curves as a function of an external out-of-plane magnetic field  $B$  allows us to reconstruct the  $I_S(\phi_1, \phi_2)$  characteristics of the bi-SQUID, where  $\phi_1$  and  $\phi_2$  are the magnetic fluxes threading loops 1 and 2, respectively [see Fig. 1(a)]. The  $I_S(B)$  of a representative device is shown in Fig. 2(a) for selected temperatures ranging between 30 mK and 700 mK. Critical-current modulation is present up to approximately 850 mK, with a modulation visibility.  $v = 2(I_{S_{\text{max}}} - I_{S_{\text{min}}})/(I_{S_{\text{max}}} + I_{S_{\text{min}}})$  ranging from approximately 52% (at 30 mK) to approximately 75% at (700 mK).  $v$  is plotted versus the temperature  $T$  in Fig. 2(b).

Similarly as for single-loop *S-N-S* interferometers, due to the contribution to the total flux of the second loop and also to the presence of a sufficiently small junction capacitance ( $C$ ), the bi-SQUID current-flux relation can still be described within the framework of the RSJ model [1]. However, the behavior observed for bi-SQUIDs deviates significantly from those observed in conventional dc SQUIDs. Indeed, the RSJ model, although conceived for Josephson tunnel junctions, retains its validity for weak

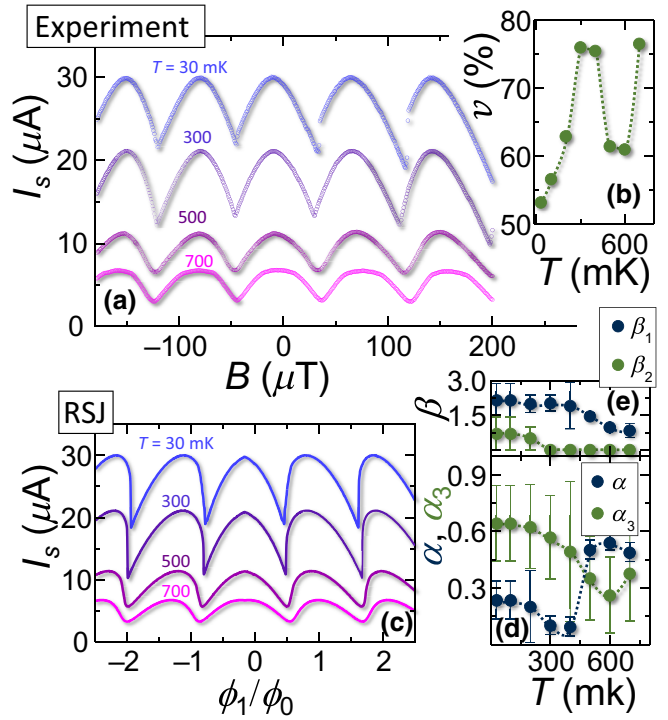


FIG. 2. The switching current versus the flux characterization of the *S-N-S* SQUID. (a) The switching current  $I_S$  of the bi-SQUID as a function of the out-of-plane magnetic field  $B$  for selected bath temperatures ranging from 30 mK to 700 mK. The external out-of-plane magnetic field is applied through a superconducting electromagnet.  $I_S(B)$  is shown for selected temperatures ranging between 30 mK and 700 mK. (b) The critical-current modulation visibility  $v = 2(I_{S_{\text{max}}} - I_{S_{\text{min}}})/(I_{S_{\text{max}}} + I_{S_{\text{min}}})$  versus the temperature  $T$ . (c) A plot of the numerical  $I_S(\phi)$  obtained through a resistively shunted junction (RSJ) fit of the experimental data of Fig. 2(a). (d) The asymmetry parameters  $\alpha$  (blue dots) and  $\alpha_3$  (green dots) as a function of the temperature. The error bars represent the 95% confidence bound for the parameter value returned by the fit procedure. (e) The screening parameters  $\beta_1$  (blue dots) and  $\beta_2$  (green dots) as a function of the temperature. The values reported in (d) and (e) are extracted through the fitting procedure (see text). The error bars represent the 95% confidence bound for the parameter value returned by the fit procedure.

links with a sinusoidal current-phase relation like that of long *S-N-S* junctions and can, therefore, be adapted to our *S-N-S* bi-SQUID circuit by merely including the equations accounting for magnetic flux quantization on both the loops as follows:

$$i = I_0[(1 + \alpha) \sin(\delta_A) + (1 - \alpha) \sin(\delta_B)], \quad (1)$$

$$\begin{aligned} \delta_C &= \pi\beta_1 j_1 - 2\pi\phi_1/\phi_0 = \pi\beta_1 j_2 - 2\pi\beta_1\alpha_3 \sin(\delta_c) \\ &\quad - 2\pi\phi_1/\phi_0, \end{aligned} \quad (2)$$

$$\delta_C = \delta_B - \delta_A + 2\pi\phi_2/\phi_0 - \pi\beta_2 j_2, \quad (3)$$

where  $\phi_0 \simeq 2.067 \times 10^{-15}$  Wb is the magnetic flux quantum,  $\alpha = I_A - I_B/I_A + I_B$  describes the asymmetry between the critical currents  $I_A$  and  $I_B$  of the two Josephson junctions  $A$  and  $B$ ,  $I_0 = I_A + I_B/2$  corresponds to one half the critical current of the interferometer (i.e., the average critical current of junctions  $A$  and  $B$ ), and  $\alpha_3 = I_C/I_0$  accounts for the critical current  $I_C$  of the third junction.  $\delta_{A,B,C}$  are the phase differences across the weak links, while  $i$  and  $j_{1,2}$  are the supercurrent passing through the bi-SQUID and the current circulating in loops 1 and 2, respectively. Finally, through the screening parameter  $\beta_{1,2}$ , the ring inductances are accounted for [1]. The  $I_S(B)$  curves are fitted [41,44] through the RSJ model by a least-squares fit procedure that minimizes the distance between the experimental data and the device theoretical switching current, calculated as a function of the fit parameters. The theoretical value of  $I_S$  is numerically determined by solving the system of Eqs. (1)–(3) in the junction phase drops versus the bias current ( $i$ ) and then maximizing  $i$  over the phase drops. This allows us to extract the relevant device parameters at 30 mK, such as the effective loop areas (approximately  $22 \pm 0.7 \mu\text{m}^2$  and approximately  $2 \pm 0.7 \mu\text{m}^2$ ), the asymmetry parameters ( $\alpha = 0.23 \pm 0.1$  and  $\alpha_3 = 0.6 \pm 0.2$ ), and the screening parameters ( $\beta_1 = 2.1 \pm 0.7$  and  $\beta_2 = 0.7 \pm 0.7$ ). Such values are in agreement with the design of our *S-N-S* bi-SQUID. Their evolution with temperature is shown in Figs. 2(d) and 2(e). Both  $\beta_1$  and  $\beta_2$  decay with the temperature due to the decay of the critical current of the junctions. In particular,  $\beta_2$  becomes negligible at approximately 300 mK, due to the faster decay of  $I_C$  with respect to  $I_A$  and  $I_B$ . This fact is confirmed by the behavior of  $\alpha_3$  versus  $T$ , which decreases from the value of approximately 0.6 to about 0.3 at 600 mK. The  $I_S(\phi_1)$  curves calculated from the fitting procedure are shown in Fig. 2(c) (note that  $\phi_2$  is just proportional to  $\phi_1$ ). All of this confirms the ability of the RSJ model to successfully capture the essential physical aspects that are in play in these devices.

We now discuss the performance of our *S-N-S* bi-SQUID in view of its possible exploitation as a linear-response magnetic flux sensor operating in the dissipative regime, which is realized by current biasing the interferometer across or above its switching current at a fixed magnetic field working point. The modulation of the magnetic flux is transduced into a change of the voltage drop  $V$  developed at the ends of the interferometer.

Within the RSJ framework, it is possible to deduce the  $V(\phi) = R_N \sqrt{I^2 - I_S^2}$  voltage response curve [1] at constant current bias  $I$ , through knowledge of the device switching-current versus flux characteristics and the device total resistance in the normal state,  $R_N$ . Figure 3(a) shows the  $V(\phi)$  values extracted from the numerical curve  $I_S(\phi_1)$  at 30 mK [see Fig. 2(c)] for selected values of the normalized bias current  $I/2I_0$ . Such theoretical  $V(\phi_1)$  curves are

significantly different from those of conventional SQUIDs, showing, indeed, a *shark-fin* voltage oscillation in the flux, for a current bias above the switching current. At lower bias currents, zero-voltage-drop regions are observed for magnetic fluxes and bias currents such that  $I < I_S(\phi_1)$ . This results in a strongly nonlinear behavior at the switching points and in the quasilinear regime in the finite-resistance regions. In the latter, the effective linearity can be quantified by the figure of merit of the total harmonic distortion (THD) [48], which is defined here as  $L(\bar{\phi}) = -20 \log(\sqrt{\sum_{n=2}^{\infty} A_n^2/A_1})$ , and which is calculated at a fixed working point  $\bar{\phi}$  through the Fourier transform  $A_0 + \sum_{n=1}^{\infty} A_n \sin(\omega_n t)$  of the device voltage response  $V[\phi_1(t)]$  to a periodic sinusoidal modulation of the magnetic flux of amplitude  $\Phi$ , such that  $\phi_1(t) = \bar{\phi} + \Phi \sin(\omega_1 t)$ , where  $t$  is the time coordinate [see the inset of Fig. 4(b)]. Such a method, which is valid in the  $\omega_1 \rightarrow 0$  limit, yields a theoretical maximum value for  $L$  ranging from approximately 70 dB (at  $I_B/I_0 = 0.85$ ) to approximately 120 dB (at  $I_B/I_0 = 1.3$ ), for  $\Phi = \phi_0/16$ . As discussed in many other previous works [8,22–24,26,27], the inability associated with many real bi-SQUID technologies to achieve performance similar to that anticipated theoretically is a critical problem. One of the main results in this paper is that the technology that we propose enables real performance for a single bi-SQUID that is close to the theoretical performance.

The characterization of a representative bi-SQUID in the dissipative regime is reported in Fig. 3(b), where we plot the voltage drop across the device at 30 mK recorded by a four-wire lock-in technique for selected amplitudes of a 17-Hz sinusoidal current-bias signal. Similarly to the RSJ model, below  $I \sim 21.5 \mu\text{A}$  the curves exhibit a zero voltage drop for magnetic fluxes such that  $I < I_S(\phi_1)$ , while a finite  $V$  value is measured when the interferometer is driven into the dissipative regime. In the low-current-bias regime, the agreement between the model and the experimental data is just qualitative. Indeed, although the RSJ prediction grasps the overall qualitative behavior of the *S-N-S* bi-SQUID, it is not able to catch the finest details of the behavior of our *S-N-S* junctions. We guess that better agreement could be obtained through a more sophisticated model (based, e.g., on a full quasiclassical description of the interferometer [49]), which is beyond the purpose of this work. For  $I \gtrsim 21.5 \mu\text{A}$ , the device permanently operates in the latter regime, showing the same *shark-fin* behavior as observed theoretically with the RSJ model. This regime can be fully exploited up to above approximately 500 mK, with a voltage-swing amplitude increasing from approximately 15  $\mu\text{V}$  (at 500 mK) to approximately 200  $\mu\text{V}$  by lowering the temperature down to 30 mK [see Fig. 3(c)]. For temperatures lower than approximately 300 mK, the  $V(\phi_1)$  characteristics retains the *shark-fin* shape observed at 30 mK. At higher temperatures, such

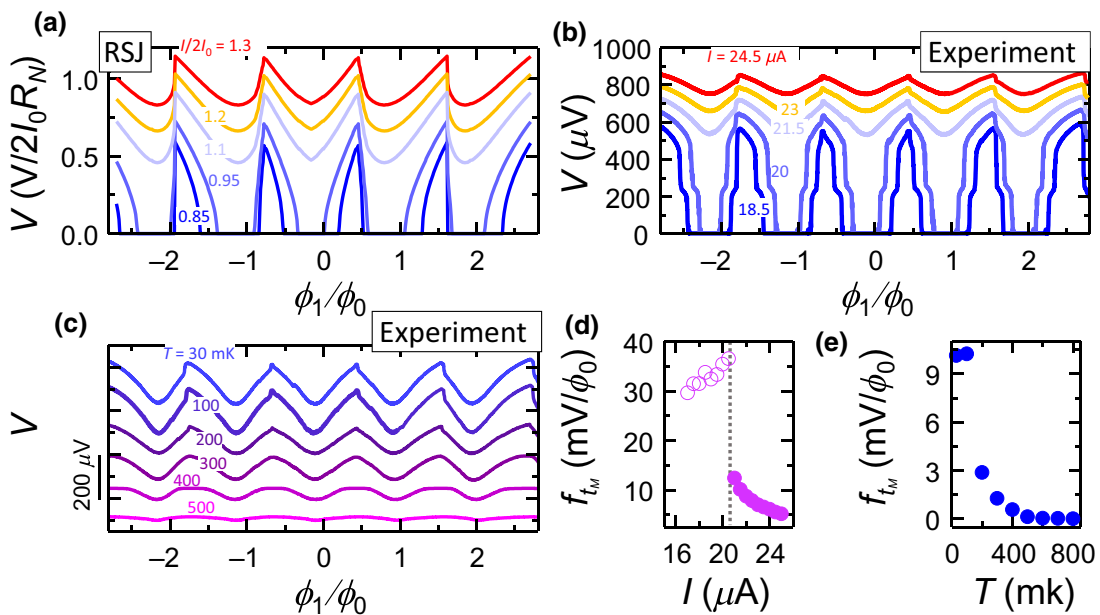


FIG. 3. A *S-N-S* bi-SQUID operated in the dissipative regime. (a) The voltage-flux response curves numerically calculated through an RSJ model ( $V(\phi_1) = R_N \sqrt{I^2 - I_S^2}$ ) at selected relative current bias  $I/I_S$ . The curves are calculated by means of the numerical  $I_S(\phi_1)$  derived from the fit of the experimental data of Fig. 2(a) at 30 mK. (b) The four-wire lock-in  $V(\phi_1)$  characteristics at 30 mK for selected values of the root-mean-square (rms) bias current  $I$  between 3  $\mu\text{A}$  and 6.4  $\mu\text{A}$ , measured by biasing the device with a 17-Hz sinusoidal current signal. Below  $I \simeq 21.5 \mu\text{A}$ , the curves show null voltage drop when  $I < I_S(\phi_1)$ . A finite  $V$  value is measured when the device is in the dissipative regime, i.e., when  $I$  is larger than the flux-dependent switching current. (c) The four-wire lock-in  $V(\phi)$  characteristics at selected temperature between 30 mK and 500 mK.  $I$  is chosen at each temperature in order to let the device operate permanently in the dissipative regime and to maximize the linearity of the voltage-flux response (see text).  $I$  is set to 21.5  $\mu\text{A}$ , 21  $\mu\text{A}$ , 20  $\mu\text{A}$ , 16  $\mu\text{A}$ , 13  $\mu\text{A}$ , and 9  $\mu\text{A}$  for  $T$  equal to 30 mK, 100 mK, 200 mK, 300 mK, 400 mK, and 500 mK, respectively. (d) The maximum value  $f_{t_M}$  of the transfer function ( $f_t$ ) versus  $I_{\text{rms}}$ . The empty circles correspond to  $f_t$  values obtained in the mixed superconductive-dissipative regime and the filled circles to the fully resistive regime. The dashed vertical gray line separates the two regimes. (e) The maximum value  $f_{t_M}$  of the transfer function ( $f_t$ ) versus  $T$ . The plotted values are obtained in the fully resistive regime.

behavior evolves into a *trapezoidal* oscillation of the voltage-versus-flux characteristics.

The conventional figure of merit of the maximum value of the transfer function  $f_{t_M}$ , calculated by looking for the maximum of the flux-to-voltage transfer function defined as  $f_t = \partial V / \partial \phi$ , is also shown in Figs. 3(d) and 3(e), respectively, as a function of  $I$  and  $T$ .  $f_{t_M}$  grows linearly as a function of the bias current up to a value of approximately 35 mV/ $\phi_0$  at approximately 20  $\mu\text{A}$ . In such a regime,  $V$  is null for some flux intervals and maxima in  $f_{t_M}$  occur at the switching points between the zero-voltage and finite-voltage regions, where high values of the flux-to-voltage transfer could, in principle, allow for highly sensitive device operation. However, the switching condition can hardly be exploited as a stable working point due the stochastic nature of the switching, which leads to a vanishing flux dynamic range. Above approximately 20  $\mu\text{A}$ , the device is instead fully resistive, resulting in a sudden drop of the transfer function and in a fast decay of  $f_{t_M}$  with the biasing current. Finally,  $f_{t_M}$  decays with the temperature from the value of 10 mV/ $\phi_0$  obtained at 30 mK and

vanishes for  $T \gtrsim 500 \text{ mK}$ . On this point, we emphasize that, in terms of the transfer function, our *S-N-S* bi-SQUID outperforms interferometers of similar typology [41,44] by 2 orders of magnitude. The measure of  $f_{t_M}$  in the fully resistive regime also allows us to provide an upper boundary for the flux noise sensitivity of the *S-N-S* bi-SQUIDs. The output voltage-noise spectral density of conventional *S-I-S* bi-SQUIDs has theoretically been shown to be comparable but yet intrinsically about twice as large as that of a dc SQUID based on the same technology, especially at low magnetic flux values [23]. This is mainly motivated by the presence of a third Josephson junction, which acts as an additional source of fluctuations, and by the nonlinear flux-to-phase-difference conversion exploited to linearize the bi-SQUID response. Although these considerations have been originally related to *S-I-S*-based bi-SQUIDs, they can reasonably be applied to *S-N-S* bi-SQUIDS as well, thus letting us assume the room-temperature voltage-amplification stage to be the limiting noise factor of our setup. Indeed, the latter introduces a voltage-noise spectral density no lower than 15 nV/ $\sqrt{\text{Hz}}$ , i.e., about one order

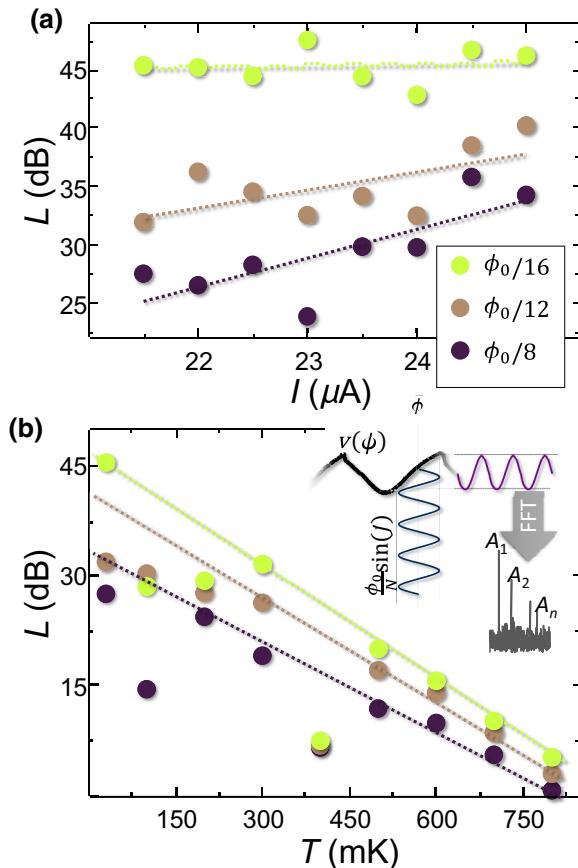


FIG. 4. The linearity of the voltage-flux response of the *S-N-S* bi-SQUIDs extracted from the experimental data. (a) The total harmonic distortion  $L = -20 \log(\sqrt{\sum_{n=2}^{\infty} A_n^2}/A_1)$  versus  $I$  for selected values of the flux-modulation amplitude  $\Phi$ , between  $\phi_0/8$  and  $\phi_0/16$ . The dashed lines are guides for the eye. (b) The temperature- $T$  evolution of the linearity  $L$ . The inset shows a schematic of the method exploited to extract  $L$  from the  $V(\phi_1)$  characteristics. A sinusoidal modulation  $\Phi \sin(\omega_1)$  of the flux around the working point  $\bar{\phi}$  with arbitrary frequency  $\omega_1/2\pi$  translates into a voltage signal through the experimental flux-to-voltage response curves [plotted in Figs. 3(b) and 3(c)]. The resulting signal is then fast Fourier transformed to compute  $L$ .

of magnitude larger than that of *S-N-S*-based mesoscopic dc SQUIDs [44]. Finally, through the ratio between the voltage-noise spectral density of our voltage preamplifier and  $f_M$ , we can calculate the upper limit for flux-noise sensitivity of our setup, which is approximately  $1\mu\phi_0/\sqrt{\text{Hz}}$ . This value is on par with the performance of commercial tunnel-junction-based SQUIDS.

Finally, we focus on the measure of the linearity of the low-frequency voltage-flux response of *S-N-S* bi-SQUIDs. This is extracted from the experimental data by following the same numerical approach as exploited to assess the THD of a sinusoidal modulation of the magnetic flux by using the  $V(\phi_1)$  RSJ characteristics and is schematically

depicted in the inset of Fig. 4(b). Figure 4(a) reports  $L$  versus  $I$  for selected values of the flux-modulation amplitude  $\Phi$ , between  $\phi_0/8$  and  $\phi_0/16$ .  $L$  exhibits a linear dependence on  $I$  and ranges between 25 dB at  $21\mu\text{A}$  (and  $\Phi = \phi_0/8$ ) and approximately 46 dB at  $25\mu\text{A}$  (and  $\Phi = \phi_0/16$ ). By decreasing the amplitude of  $\Phi$ , the average value of  $L$  is observed to increase due to the reduction of the ratio between the linear portion of the  $V(\phi_1)$  characteristics and  $\Phi$ . Furthermore, the slope of  $L$  versus  $I$  decreases by reducing the flux-modulation amplitude. This suggests that, for practical applications, at higher values of  $\Phi$  the bias current might be exploited as a variable control to increase the linearity of the device response.  $L$  persists within the range between 20 dB and 45 dB up to approximately 300 mK. Above such a threshold temperature, it decreases linearly as a consequence of the temperature evolution of the  $V(\phi_1)$ , which moves from the *shark-fin* shape to the *trapezoidal* one. We conclude this section by remarking on the relevance of the performance achieved by our *S-N-S* bi-SQUID in terms of response linearity. Indeed, the measured  $L$  values, although still far from those expected from the RSJ model, are yet very promising when compared to those of tunnel-junction-based devices composed of arrays of hundreds of interferometers [8].

### III. CONCLUSIONS

Among available magnetic field sensors, superconducting interferometers have progressively become an essential tool for a multitude of applications ranging from nanomagnetometry to telecom signal processing. Here, we discuss the implementation of a superconducting bi-SQUID based on proximitized mesoscopic Al-Cu-Al junctions. Such a design provides a viable technological alternative to the conventional approach based on tunnel JJs and holds the promise of excellent performance in terms of the transfer function as well as of the voltage-to-flux response. The latter, which we measure in the low-frequency limit, is on par with the performance obtained so far on tunnel-junction-based devices made of several tens or hundreds of bi-SQUIDS. This consideration allows us to speculate about the successful exploitation of *S-N-S* bi-SQUIDS in place of tunnel-junction-based interferometers.

### ACKNOWLEDGMENTS

We acknowledge the European Research Council under Grant Agreement No. 899315-TERASEC and the European Union Horizon 2020 research and innovation program under Grant Agreements No. 800923 (SUPERTED) and No. 964398 (SUPERGATE) for partial financial support. F.G. and G.C.T. acknowledge many useful conversations on the subject matter of this research with Dr P. Atanackovic.

## APPENDIX

## 1. Device nanofabrication

The  $S\text{-}N\text{-}S$  bi-SQUIDs are fabricated in a single electron-beam lithography (EBL) step and a two-angle shadow-mask metal deposition through a suspended PMMA-resist mask onto a  $\text{SiO}_2$  substrate. The Al-Cu  $S\text{-}N$  clean interfaces are obtained through electron-beam evaporation in an ultrahigh-vacuum (UHV) chamber with a base pressure of approximately  $5 \times 10^{-11}$  Torr. The Ti(5 nm)/Cu(25 nm) bilayer (the Ti promotes adhesion) is evaporated at an angle of  $0^\circ$  to realize the SQUID nanowires. The sample holder is then tilted at an angle of  $13^\circ$  for the deposition of a 100-nm-thick film of Al to realize the superconducting loop.

## 2. Cryogenic electrical characterization

The electrical characterization of the interferometer is carried out using a four-wire technique in a filtered cryogen-free  $^3\text{He}$ - $^4\text{He}$  dilution fridge equipped with a superconducting electromagnet. The current-voltage ( $I\text{-}V$ ) measurements are carried out by setting a low-noise current bias through a room-temperature voltage generator and a bias resistor. The voltage drop across the interferometer is measured with a room-temperature preamplifier. The switching current values are averaged over the switching points of 15 repetitions of the same  $I\text{-}V$  curve. The voltage-versus-flux characterization is performed through a low-frequency lock-in technique.

- [1] J. Clarke and A. I. Braginski, *SQUID Handbook*, edited by J. Clarke and A. I. Braginski, Vol. 1 (Wiley, 2004), p. 1.
- [2] A. Barone and G. Paternò, *Physics and Application of the Josephson Effect* (John Wiley & Sons, Inc, New York, 1982).
- [3] R. Kleiner, D. Koelle, F. Ludwig, and J. Clarke, Superconducting quantum interference devices: State of the art and applications, *Proc. IEEE* **92**, 1534 (2004).
- [4] M. J. Martínez-Pérez and D. Koelle, in *Superconductors at the Nanoscale* (De Gruyter, 2017) Chap. 11, p. 339.
- [5] C. Granata and A. Vettoliere, Nano superconducting quantum interference device: A powerful tool for nanoscale investigations, *Phys. Rep.* **614**, 1 (2016).
- [6] F. Giazotto, T. T. Heikkilä, G. P. Pepe, P. Helistö, A. Luukanen, and J. P. Pekola, Ultrasensitive proximity Josephson sensor with kinetic inductance readout, *Appl. Phys. Lett.* **92**, 162507 (2008).
- [7] R. L. Fagaly, H.-J. Krause, M. Mück, S. Tanaka, H. Nowak, R. Stolz, J. Kirtley, T. Schurig, J. Beyer, R. McDermott, W. Vodel, R. Geithner, and P. Seidel, in *Applied Superconductivity* (Wiley-VCH Verlag GmbH & Co. KGaA, Weinheim, Germany, 2015), p. 949.
- [8] V. K. Kornev, N. V. Kolotinskiy, and O. A. Mukhanov, Bi-SQUID: Design for applications, *Supercond. Sci. Technol.* **33**, 113001 (2020).
- [9] B. D. Josephson, Possible new effects in superconductive tunnelling, *Phys. Lett.* **1**, 251 (1962).
- [10] R. Doll and M. Nähauer, Experimental Proof of Magnetic Flux Quantization in a Superconducting Ring, *Phys. Rev. Lett.* **7**, 51 (1961).
- [11] B. S. Deaver and W. M. Fairbank, Experimental Evidence for Quantized Flux in Superconducting Cylinders, *Phys. Rev. Lett.* **7**, 43 (1961).
- [12] G. Prokopenko, S. Shitov, I. Lapitskaya, V. Koshelets, and J. Mygind, Dynamic characteristics of  $S$ -band dc SQUID amplifier, *IEEE Trans. Appl. Supercond.* **13**, 1042 (2003).
- [13] G. Prokopenko, S. Shitov, D. Balashov, P. Dmitriev, V. Koshelets, and J. Mygind, Low-noise  $S$ -band dc SQUID based amplifier, *IEEE Trans. Appl. Supercond.* **11**, 1239 (2001).
- [14] M. Mück and J. Clarke, Harmonic distortion and intermodulation products in the microstrip amplifier based on a superconducting quantum interference device, *Appl. Phys. Lett.* **78**, 3666 (2001).
- [15] G. Prokopenko, D. Balashov, S. Shitov, V. Koshelets, and J. Mygind, Two-stage  $S$ -band dc SQUID amplifier, *IEEE Trans. Appl. Supercond.* **9**, 2902 (1999).
- [16] G. Prokopenko, S. Shitov, V. Koshelets, D. Balashov, and J. Mygind, A dc SQUID based low-noise 4 GHz amplifier, *IEEE Trans. Appl. Supercond.* **7**, 3496 (1997).
- [17] M. Huber, P. Neil, R. Benson, D. Burns, A. Corey, C. Flynn, Y. Kitaygorodskaya, O. Massihzadeh, J. Martinis, and G. Hilton, DC SQUID series array amplifiers with 120 MHz bandwidth, *IEEE Trans. Appl. Supercond.* **11**, 1251 (2001).
- [18] M. Mück and J. Clarke, Flux-bias stabilization scheme for a radio-frequency amplifier based on a superconducting quantum interference device, *Rev. Sci. Instrum.* **72**, 3691 (2001).
- [19] M. Mück, M.-O. André, J. Clarke, J. Gail, and C. Heiden, Microstrip superconducting quantum interference device radio-frequency amplifier: Tuning and cascading, *Appl. Phys. Lett.* **75**, 3545 (1999).
- [20] M.-O. André, M. Mück, J. Clarke, J. Gail, and C. Heiden, Radio-frequency amplifier with tenth-kelvin noise temperature based on a microstrip direct current superconducting quantum interference device, *Appl. Phys. Lett.* **75**, 698 (1999).
- [21] M. Mück, M.-O. André, J. Clarke, J. Gail, and C. Heiden, Radio-frequency amplifier based on a niobium dc superconducting quantum interference device with microstrip input coupling, *Appl. Phys. Lett.* **72**, 2885 (1998).
- [22] V. K. Kornev, I. I. Soloviev, N. V. Klenov, A. V. Sharafiev, and O. A. Mukhanov, Linear bi-SQUID arrays for electrically small antennas, *IEEE Trans. Appl. Supercond.* **21**, 713 (2011).
- [23] V. K. Kornev, A. V. Sharafiev, I. I. Soloviev, and O. A. Mukhanov, Signal and noise characteristics of bi-SQUID, *Supercond. Sci. Technol.* **27**, 115009 (2014).
- [24] V. K. Kornev, I. I. Soloviev, N. V. Klenov, and O. A. Mukhanov, Bi-SQUID: A novel linearization method for dc SQUID voltage response, *Supercond. Sci. Technol.* **22**, 114011 (2009).
- [25] A. Sharafiev, I. Soloviev, V. Kornev, M. Schmelz, R. Stolz, V. Zakosarenko, S. Anders, and H.-G. Meyer, Bi-SQUIDS

- with submicron cross-type Josephson tunnel junctions, *Supercond. Sci. Technol.* **25**, 045001 (2012).
- [26] V. K. Kornev, N. V. Kolotinskiy, A. V. Sharafiev, I. I. Soloviev, and O. A. Mukhanov, Broadband active electrically small superconductor antennas, *Supercond. Sci. Technol.* **30**, 103001 (2017).
- [27] V. K. Kornev, N. V. Kolotinskiy, A. V. Sharafiev, I. I. Soloviev, and O. A. Mukhanov, From single SQUID to superconducting quantum arrays, *Low Temp. Phys.* **43**, 829 (2017).
- [28] K. K. Likharev, Superconducting weak links, *Rev. Mod. Phys.* **51**, 101 (1979).
- [29] R. Vijay, E. M. Levenson-Falk, D. H. Slichter, and I. Siddiqi, Approaching ideal weak link behavior with three dimensional aluminum nanobridges, *Appl. Phys. Lett.* **96**, 223112 (2010).
- [30] E. M. Levenson-Falk, R. Vijay, N. Antler, and I. Siddiqi, A dispersive nanoSQUID magnetometer for ultra-low noise, high bandwidth flux detection, *Supercond. Sci. Technol.* **26**, 055015 (2013).
- [31] F. Giazotto, K. Grove-Rasmussen, R. Fazio, F. Beltram, E. H. Linfield, and D. A. Ritchie, Josephson current in Nb/InAs/Nb highly transmissive ballistic junctions, *J. Supercond.* **17**, 317 (2004).
- [32] F. Carillo, G. Biasiol, D. Frustaglia, F. Giazotto, L. Sorba, and F. Beltram, In<sub>0.75</sub>Ga<sub>0.25</sub> As on GaAs submicron rings and their application for coherent nanoelectronic devices, *Phys. E Low-Dimens. Syst. Nanostruct.* **32**, 53 (2006).
- [33] F. Giazotto, P. Spathis, S. Roddaro, S. Biswas, F. Taddei, M. Governale, and L. Sorba, A Josephson quantum electron pump, *Nat. Phys.* **7**, 857 (2011).
- [34] A. M. Savin, J. P. Pekola, J. T. Flyktman, A. Anthore, and F. Giazotto, Cold electron Josephson transistor, *Appl. Phys. Lett.* **84**, 4179 (2004).
- [35] B. Pannetier and H. Courtois, Andreev reflection and proximity effect, *J. Low Temp. Phys.* **118**, 599 (2000).
- [36] W. Belzig, F. K. Wilhelm, C. Bruder, G. Schön, and A. D. Zaikin, Quasiclassical Green's function approach to mesoscopic superconductivity, *Superlattices Microstruct.* **25**, 1251 (1999).
- [37] W. L. McMillan, Tunneling model of the superconducting proximity effect, *Phys. Rev.* **175**, 537 (1968).
- [38] T. T. Heikkilä, J. Särkkä, and F. K. Wilhelm, Supercurrent-carrying density of states in diffusive mesoscopic Josephson weak links, *Phys. Rev. B* **66**, 184513 (2002).
- [39] J. J. A. Baselmans, A. F. Morpurgo, B. J. van Wees, and T. M. Klapwijk, Reversing the direction of the supercurrent in a controllable Josephson junction, *Nature* **397**, 43 (1999).
- [40] G. De Simoni, F. Paolucci, C. Puglia, and F. Giazotto, Josephson field-effect transistors based on all-metallic Al/Cu/Al proximity nanojunctions, *ACS Nano* **13**, 7871 (2019).
- [41] G. De Simoni, S. Battisti, N. Ligato, M. T. Mercaldo, M. Cuoco, and F. Giazotto, Gate control of the current-flux relation of a Josephson quantum interferometer based on proximitized metallic nanojunctions, *ACS Appl. Electron. Mater.* **3**, 3927 (2021).
- [42] G. C. Tettamanzi, I. Nakone, F. Giazotto, and P. Atanackovic, Australian Patent Application No. 2020904035 (2020).
- [43] L. Angers, F. Chiodi, G. Montambaux, M. Ferrier, S. Guéron, H. Bouchiat, and J. C. Cuevas, Proximity dc SQUIDs in the long-junction limit, *Phys. Rev. B* **77**, 165408 (2008).
- [44] A. Ronzani, M. Baillergeau, C. Altimiras, and F. Giazotto, Micro-superconducting quantum interference devices based on V/Cu/V Josephson nanojunctions, *Appl. Phys. Lett.* **103**, 052603 (2013).
- [45] A. Ronzani, C. Altimiras, and F. Giazotto, Balanced double-loop mesoscopic interferometer based on Josephson proximity nanojunctions, *Appl. Phys. Lett.* **104**, 032601 (2014).
- [46] H. Courtois, M. Meschke, J. T. Peltonen, and J. P. Pekola, Origin of Hysteresis in a Proximity Josephson Junction, *Phys. Rev. Lett.* **101**, 067002 (2008).
- [47] P. Dubos, H. Courtois, B. Pannetier, F. K. Wilhelm, A. D. Zaikin, and G. Schön, Josephson critical current in a long mesoscopic S-N-S junction, *Phys. Rev. B* **63**, 064502 (2001).
- [48] I. I. Soloviev, V. I. Ruzhickiy, N. V. Klenov, S. V. Bakurskiy, and M. Y. Kupriyanov, A linear magnetic flux-to-voltage transfer function of a differential dc SQUID, *Supercond. Sci. Technol.* **32**, 074005 (2019).
- [49] K. D. Usadel, Generalized Diffusion Equation for Superconducting Alloys, *Phys. Rev. Lett.* **25**, 507 (1970).

*Correction:* The author order was presented incorrectly and has been fixed.